Thermal water splitting on the WO3 surface-experimental proof

Anna Staerz, Arne Kobald, Tamara Russ, Udo Weimar, Anne Hémeryck,
Nicolae Barsan

THERMAL WATER SPLITTING ON THE WO$_3$ SURFACE-EXPERIMENTAL PROOF

Anna Staerz[1], Arne Kobald[1], Tamara Russ[1], Udo Weimar[1], Anne Hémeryck[2] and Nicolae Barsan[1,*]

[1]Faculty of Science, Department of Chemistry, Institute of Physical and Theoretical Chemistry, Tuebingen University, Auf der Morgenstelle 15, 72076 Tuebingen, Germany

[2]LAAS-CNRS, Université de Toulouse, CNRS, 31400 Toulouse, France

ABSTRACT: Here, the splitting of water from humidity at the surface of WO$_3$ is reported. The production of hydrogen occurs under mild conditions, at 300 °C in the presence of humidity. Using operando diffuse reflectance infrared Fourier transform spectroscopy and DC resistance measurements complemented with DFT calculations, it was possible to elucidate the temperature dependent surface reactions of WO$_3$ with humidity. By examining multiple different nanomaterials at 300°C, it was found that the oxidation of the surface by humidity is generally valid for WO$_3$. The evolution of hydrogen was detected using catalytic conversion measurements. In addition to the evolution of hydrogen, understanding the interaction between the surface and humidity is a prerequisite for the optimized use of WO$_3$ for a wide array of applications, such as optical sensors or memristors.

Introduction

WO$_3$ is an n-type semiconductor with a number of interesting characteristics, making it a versatile material that is widely used. Already in the 1960s, Deb et al. found that WO$_3$ is electrochromic.[1] The electrochromic process of WO$_3$ is the change in color associated with the loss/gain of a proton/electron due to a small applied voltage.[1] In addition, WO$_3$ is known to be gasochromic; through modification with noble metals the direct insertion of hydrogen via a spillover effect is reported in literature. The resulting formation of tungsten bronzes, A$_x$WO$_3$ where A$^+$ is a small ion, e.g. H$^+$, leads to the reduction of W^{6+} to W^{5+}.[2] As a result of the changed oxidation state of tungsten, the bronzes adsorb photons in the visible region. The degree of coloration is found to be dependent on the atmospheric concentration of hydrogen.[3] This has been used for the development of optically-based hydrogen sensors.[3] The effect of atmospheric humidity on the coloration of WO$_3$ is, however, poorly understood and reports are even conflicting.[4,5] While it is thought that adsorbed water is key for its photochromic properties (light activated chromism), humidity reportedly decreases the sensitivity of optical hydrogen detectors.[4,6,7] Also, the memristive qualities of WO$_3$ are found to increase in the presence of background humidity.[8] Although it is usually assumed that the memristive properties of WO$_3$ is induced by the migration of oxygen vacancies, Zhou et al. hypothesize purely based on I-V curves that the enhancement is a result of H$^+$ ions stemming from oxidized water drifting on the surface of a WO$_3$ nanowire via the Grotthuss mechanism.[8]

Despite the vast amount of research done on WO$_3$ across the many application fields, the reactions between the surface and the atmosphere are still poorly understood. Specifically, despite its omnipresence in applications, the interaction between humidity and the WO$_3$ surface remains unclear. It is known for porous films made of semiconducting metal oxide (SMOX) nanopowder, in general, that the reaction between the atmospheric gas and the surface of the grains results in a detectable change of the resistance.[9,10] In the case of an n-type material like WO$_3$ operated at 300 °C, an increase of the resistance is expected for oxidizing gases and a decrease in the presence of humidity.[11-13] For porous films of WO$_3$, however, the increase of the baseline resistance, at an operation temperature of 300 °C in the presence of humidity, has been reported.[14,15] Humidity reduces the response of WO$_3$ chemiresistive gas sensors to oxidizing gases, e.g. NO$_2$ and ozone.[15-17] Based on preliminary measurements, the competing reactions of humidity and oxidizing gases has been given as a tentative explanation.[15,18,19] A similar mechanism was recently reported by Daeneke et al. for the interaction of molybdenum sulfide and titanium oxide ink with atmospheric humidity under light irradiation.[20] As the ink can be coated onto any substrate, the hydrogen production from humidity is arguably easy and inexpensive.[20]

WO$_3$ is also a promising material for use in photoelectrochemical or photocatalytic water splitting. In the context of this application, Albanese et al. and Teusch et al. have theoretically examined the interaction of water with WO$_3$. Both very recent studies, find that molecular H$_2$O easily adsorbs onto surface tungsten sites. Albanese et al. concluded that the reaction of the WO$_3$ surface with hydrogen could easily result in surface oxygen vacancies.[21] Similarly, Teusch et al. found that the water splitting process does not take place without external influences due to the strong adsorption of hydrogen.[22] Kishore et al. modelled the oxygen evolution reaction (OER), which is found to account for most of the overpotential in photoelectrochemical water splitting with WO$_3$.[23] Although these studies offer an interesting basis for understanding the interaction of water with the WO$_3$ surface, they are limited to theory.

The studies were also tailored to photoelectrochemical or photocatalytic water splitting, where WO$_3$ is immersed in an electrolyte solution. As a result, the interaction of the surface

with molecular oxygen and gaseous water from the atmosphere is not considered. Additionally, only the low temperature γ-phase of WO_3 was considered. Based on their results Teusch et al. even concluded that the conditions examined in the study presented here are more fitting to those most likely required for water splitting on WO_3, at an elevated temperature (ca. 300 °C, β-phase) and in humidity (gaseous water). [22]

The presented work serves as a crucial missing link between existing theoretical and experimental literature. Water splitting on the surface of WO_3 was experimentally identified using operando diffuse reflectance infrared Fourier transform (DRIFT) spectroscopy and resistance measurements coupled with exhaust measurements. Through a systematic temperature study, complemented with information from DFT calculations, it is possible to clarify several aspects of the interaction between the WO_3 surface and humidity.

The justification of this research is twofold. The evolution of hydrogen from WO_3 at 300 °C (much lower than the temperature typically used for thermochemical water splitting) as a result of humidity exposure would be remarkable.[24,25] In addition, however, it is vital for a wide array of applications, to fully understand the interaction between the WO_3 surface and humidity.

Experimental

Film Preparation: Films were made based on commercially available nanopowder (< 100 nm, Sigma Aldrich). The powders were mixed with 1,2-propanediol (Sigma-Aldrich, 99.5+% ACS reagent) and ground with mortar and pestle into a viscous paste which was printed (EKRA Microtronic II) onto alumina substrates containing platinum electrodes and a backside platinum heater (300 μm electrode gap, 300 μm width and 5 μm thickness; Ceramtec AG). The films were dried at room temperature for 1 h, overnight at 80 °C (Heraeus UT12) and then annealed for 10 min each at 400−500−400 °C in a tubular furnace (Heraeus ROK 6/30). Based on the geometry of the screen, a final film thickness of 50 μm is achieved. The sensitive layers were characterized using a JOEL JSM-6500F Scanning Electron Microscopy (SEM) with an acceleration of 15 kV, a probe current of 7 and a stage height of 10 mm.

The X-ray diffraction measurements of the heated films under humidity exposure were done using a BRUKER D8 discover GADDS microdiffractometer equipped with a Co-X-ray tube, HOPG-primary monochromator, X-ray optics and a large two dimensional VANTEC-500 detector covering 40° 2Θ, 40° 2θ and 40° ψ allowing fast and locally resolved measurements of the film.[15,26]

DC Resistance Measurements and Operando DRIFT Spectroscopy: The films are mounted into a homemade Teflon chamber and heated using an Agilent E3614A DC power supply. The gas flow was regulated using a computer monitored mass flow controller unit. The resistance was monitored using a Keithley 6517B electrometer. In order to ensure that the desired conditions were created, the exhaust gas of the resistance measurements was monitored a HYT939 humidity and temperature monitor (IST AG, Switzerland). An example of the received output is plotted in S1**Error! Reference source not found.**.

For the operando DRIFT spectra, a Vertex80v with a midband mercury cadmium telluride (MCT) detector (Bruker, Billerica, MA, USA) and a spectral resolution of 4 cm^{-1} was used. The films were mounted in a homemade chamber with a KBr window. The films were heated and their resistance was monitored simultaneously. A single-channel spectrum was recorded every 15 min. The absorbance spectra was calculated using the relation

$$\text{Absorbance} = -\log\left(\frac{\text{single channel test gas}}{\text{single channel reference}}\right) \qquad \text{eq. 1}$$

In this case the ratio between the single channel in a test gas to one taken during exposure to a reference background is considered to be the relative transmission.[27]

Operando diffuse reflectance infrared Fourier transform spectroscopy, is widely used in the catalysis and gas sensor field for the insitu studies of surface chemistry. By referencing a spectrum taken during exposure to a certain atmosphere (e.g. oxygen containing synthetic air) to a spectrum taken of the sample while in an atmosphere lacking the target gas (e.g. nitrogen), it is possible to identify the vibrational wavenumbers of surface species which change as a result of the gas exposure. In their study, Sirita et al. examined the various functions derived from the signal collected by DRIFTS used to evaluate the surface coverage of adsorbates. The authors found that the method of Olinger and Griffiths, yields the most accurate results when dealing for systems showing baseline drifts. [27,28] The ratio between the reflected intensity of the sample divided by the intensity of the reference state (I_∞(sample)/ I_∞(reference) is then taken as an approximate value for absolute reflectance R_∞. A linear representation of an adsorbate concentration is attained with log(1/R), noted "absorbance" (analogy with the absorbance log (1/T)). [27,28]

Theoretical Calculations: The periodic spin polarized calculations were performed using DFT based on the generalized gradient approximation (GGA) employing the Perdew–Burke–Ernzerhof (PBE) exchange−correlation functional as implemented in the plane-waves program Vienna Ab initio Simulation Package (VASP).[29–32] The projector-augmented wave (PAW) potentials were applied for the core electron representation.[33,34] A converged value of E_{cut} = 500 eV was used as the cutoff energy of the plane wave. The integration in reciprocal space was performed with a Monkhorst−Pack grid.[35] A k-point mesh of (4 × 4 x 1) was used. The stoichiometric (001) β-WO_3 surface was modeled by the periodic slab shown in Figure 4. The p($\sqrt{2}$x$\sqrt{2}$)-R45° cell is composed of a total number of 128 atoms with 32 W- and 96 O-atoms, corresponding to a ~10.5 Å x 10.5 Å surface and four layers. A vacuum zone of 15 Å in the z/c direction was used to create a surface effect. As detailed in Albanese and coworkers' paper[21] all the atoms are fully relaxed. We checked that bond length variations fit with trends given in the work of Albanese et al. [21] The energy of oxygen vacancy formation ΔE_O was calculated using the following relation

$$\Delta E_O = E_{vac} + \frac{1}{2}E_{O_2} - E_{surface} \qquad \text{eq. 2}$$

and the adsorption energies are calculated using the following formula:

$$\Delta E_{ads} = E_{adsorbed\ molecule} - E_{surface} - E_{gaseous\ molecule} \qquad \text{eq. 3}$$

where E_{vac} is the energy of the surface with one terminal oxygen vacancy, E_{O_2} is the energy of the isolated spin polarized O_2, $E_{surface}$ is the total energy of the relaxed surface, $E_{gaseous\ molecule}$ is the total energy of the isolated gaseous

molecule and $E_{adsorbed\ molecule}$ is the total energy of the system with a gaseous molecule adsorbed.

To calculate atomic charges and charge transfers, Bader's analysis was adapted.[36] The charge transfer is the sum of changes in charge for all atoms associated with the reference surface. Here, the reference is the slab with a terminal oxygen vacancy, V_0^C. The common DFT+U approach was found to have an insignificant effect on the charge transfers (see S2). The visualization of the cell was done using VMD.[37] Pictures were then rendered using POV-Ray.[38]

Catalytic Conversion Measurements: To gain information about the catalytic activity of WO_3 with humidity, 1 g of the commercially available nanopowder from Sigma Aldrich (<100 nm) was filled into a quartz tube (fixed with quartz wool). The tube was then heated to 300 °C using an oven (Thermicon controlled Hereaus reactor). Using a computer monitored mass flow controller unit, dry synthetic air was passed through the heated WO_3 for 3 h, followed by air at 10 % RH (attained using a water bubbler) for 2 h at a constant total flowrate of 150 ml/min. A schematic of the catalytic conversion setup is shown in Figure 1.
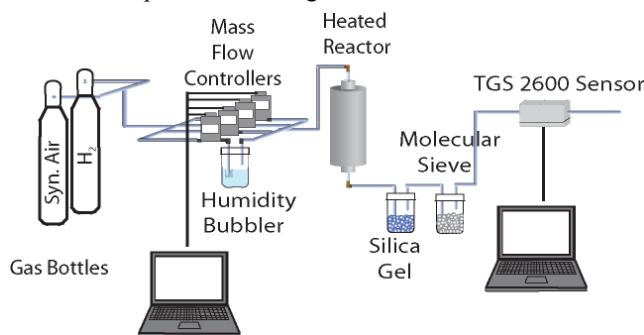

Figure 1. Setup of the catalytic conversion measurements. 1 g of WO_3 powder was heated to 300 °C and then exposed to 10% RH. The exhaust was dried using silica gel and molecular sieve and then monitored using a TGS2600 (Figaro Engineering Inc., Japan) metal oxide sensor. Reprinted with permission from Anna Staerz, from ref 39.

The measurement was repeated two times. The exhaust of the measurement was then dried using silica gel and molecular sieve before being analyzed by a metal oxide based gas sensor that is highly sensitive to H_2 (TGS2600, FIGARO Engineering Inc.). The sensor's response to hydrogen was verified by exposing the sensor to different H_2 concentrations. It was verified that the drying process was efficient and that the sensor's response was not affected by residual humidity as no response was seen if WO_3 was replaced by heated quartz wool.

Results

It is known that the reaction between the atmosphere and the surface of the grains results in a detectable change of the resistance.[9,10] Simplistically, under normal operation conditions, it is considered that atmospheric oxygen reacts with the surface of the metal oxides. The oxygen then traps electrons at the surface of the grains, resulting in an increase of the resistance for n-type semiconducting metal oxides. For WO_3, this mechanism can be verified using operando DRIFT spectroscopy. Simultaneously to resistance measurements, infrared spectra are taken of a heated sample during exposure to different atmospheres. In order to gain insight into the surface reaction, the single channel spectrum taken in synthetic air (taken during the fifteen minutes highlighted in blue in Figure 2) is then referenced to a spectrum taken of the sample in nitrogen

(taken during the fifteen minutes highlighted in red in Figure 2). According to the work of Olinger and Griffiths, this ratio represents a relative transmission and can be converted into the absorbance by taking the negative logarithm, see Figure 2. In the absorbance spectra, bands that are decreasing are associated with surface groups that are leaving the surface as a result of the gas while increasing bands belong to surface groups which are more readily present. A schematic showing how the absorbance spectrum for synthetic air was attained is shown in Figure 2.
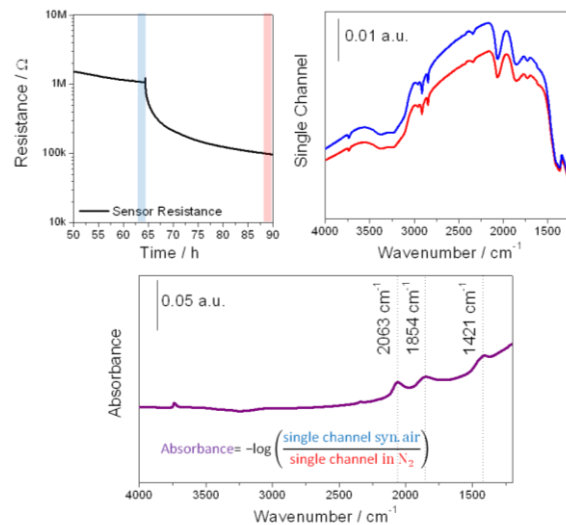

Figure 2. Resistance measurement and simultaneously attained single channels spectra of a WO_3 film during exposure to dry synthetic air (blue) and nitrogen (red) at 300 °C. By referencing the single channel spectrum in dry synthetic air to the one in nitrogen, the absorbance spectrum was attained.

The absorbance spectrum verifies the assumed surface reaction of the WO_3 film with atmospheric oxygen. In literature the bands at 2063 cm^{-1} and 1854 cm^{-1} are attributed to tungsten–oxygen bonds.[40] In the absorbance spectra, these bands are increasing indicating, as expected, that the surface is more oxidized in synthetic air than in nitrogen. Additionally the band at 1421 cm^{-1}, is found to be increasing and is therefore attributed to tungsten-oxygen, in line with a large DRIFT study on films produced from differently prepared WO_3 samples.[14] Overall, the DRIFT spectrum in synthetic air supports the general assumption that the WO_3 surface is oxidized by atmospheric oxygen. The results are helpful for the interpretation of the absorbance spectra under humidity exposure.

For most n-type semiconducting metal oxides, e.g. SnO_2 and In_2O_3, humidity is known to result in a decrease of the films resistance at 300 °C. In the case of WO_3, however, an increase of the baseline resistance in the presence of humidity has been reported.[14,15,19] When referenced to nitrogen, the bands attributed to tungsten-oxygen bonds are increasing during humidity exposure, similarly to dry synthetic air, for the WO_3 film at 300 °C see Figure 3.[37] Furthermore, the formation of hydroxyl groups is not visible.

This finding indicates a direct oxidation of the WO_3 surface by humidity. In order to verify these findings and gain insight into how water oxidizes the WO_3 surface, a temperature study was done. The resistance measurements were done on four identically prepared WO_3 films. The films were heated between 100 and 300 °C. Unexpectedly, under 175 °C, the resistance of the films significantly decreases in the presence of

humidity (Figure 3a, blue region). At mid-range temperatures around 200 °C (Figure 3a, purple region), the effect of humidity on the resistance is negligible. Above 250 °C, the resistance of the films is found to increase in the presence of humidity (Figure 3a, red region).
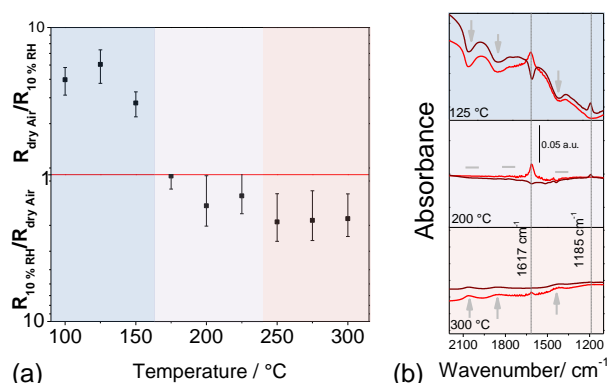

Figure 3. (a) The relative change in the resistance as a result of exposure to 10 % RH. The average of four identically prepared films was taken and the standard deviation was calculated. (b) The DRIFT spectra taken of the film at three different temperatures (125, 200, and 300 °C) during exposure first to 10 % RH (H_2O, light red) followed by 10 % RH (D_2O, dark red). The reference state was the spectrum taken in dry synthetic air.

Operando DRIFT spectra taken in 10 % RH referenced to dry synthetic air at the different temperatures provide insight into why the effect of humidity on the resistance changes over the temperature range. The most significant change is seen between 2500 and 1200 cm^{-1}, for a complete overview of the spectra please see supplementary information S2.

Overall the change of the bands attributed to the tungsten oxygen bonds correlates well to the change in resistance. At 300 °C, these bands are increasing associated with an increase in the resistance. At mid-range temperatures, around 200 °C, the resistance is largely humidity independent and no significant changes in the bands belonging to tungsten-oxygen are visible. In line with the significant decrease in the resistance of the material, at 125 °C the bands (2063 and 1854 cm^{-1}) attributed to tungsten oxygen bonds are decreasing. The formation of hydroxyl groups is not visible in the DRIFT spectrum, S3. An increasing band at around 1617 cm^{-1} is, however, visible. In literature this band is attributed to the bending mode of surface adsorbed water.[40] This designation was verified using a H_2O/D_2O experiment. A DRIFT spectrum taken during a pulse of D_2O after H_2O exposure was referenced to dry air. As expected, the exchange of H_2O with D_2O has no effect on the bands attributed to tungsten-oxygen. The band at 1617 cm^{-1}, however, decreases and a new increasing band at 1185 cm^{-1} becomes visible. This shift is in line with surface adsorbed H_2O being replaced by D_2O.

DRIFT spectroscopy is known to be a very surface sensitive method and at the examined film temperatures, it is probable that the observed reactions are surface based.[41] It is known, however, that water can be integrated into the lattice of WO_3 resulting in the formation of hydrates.[42] Here, no hydrate formation is visible in the in operando XRD, see S4**Error! Reference source not found.**, even after hours at high humid-

ity. This verifies that the process doesn't occur in the bulk of the material but is surface based.

In order to understand the charge transfer associated with the identified surface reactions, DFT calculations were done. It is known that WO_3 has different temperature dependent crystal structures.[43–46] For bulk WO_3 the phase transition between the monoclinic γ-phase and the orthorhombic β-phase occurs at temperature above 400 °C. The transition, however, has been found to occur at lower temperatures (237 °C) for nanomaterials.[45,47] The XRD spectra of the γ- and β-phase are very similar, but a splitting of the reflex at ca. 39° could indicate that the presence of both phases, see S5. To address both phases the results attained here for the stoichiometric (001) β-WO_3 surface were compared to the theoretical work of Albanese et al., Teusch et al. and Jin et al. for the γ-phase.[21,22,48]

Here, an oxygen terminated surface is considered, in which every other tungsten is 5-fold-coordinated (W_{5c}). In their work, Teusch and Klüner only considered the adsorption of water onto W_{5c}. Albanese et al. attributed the n-type conductivity of WO_3 to surface oxygen vacancies.[21] In the relaxed slab, the bond between the terminal oxygen and tungsten has a length of 1.71 Å, see Figure 4. This oxygen is stable singly charged with one excess electron.[21,48] In literature, the dominant surface vacancy (V_0^C) is found to result from the loss of O_{1C}^C.[21,48] The WO_3 films show n-type behavior, and the surface of the films is in constant equilibrium with the atmosphere. In other words, the V_0^C vacancies are in constant equilibrium with gaseous species in the atmosphere, e.g. water and oxygen. For completeness, the adsorption of oxygen and water molecularly onto both the W_{5c} and into the V_0^C is therefore considered.
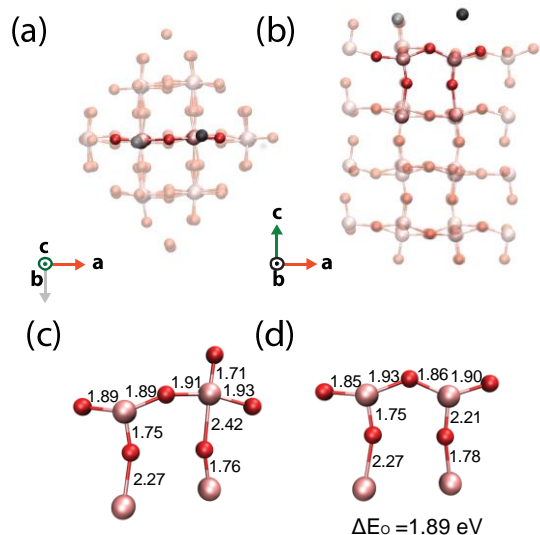

Figure 4. (a) Top-and (b) side view of the optimized (001) β-WO_3 surface with a V_0^C represented in black and an adsorption position over the W_{5c} marked in gray. A cutout of the examined W_{5c} and V_0^C of the cell (c) perfect surface and with (d) vacancy. Tungsten atoms are ochre and oxygen atoms red. Bond lengths and distances are given in Å.

The adsorption energy and charge transfer of water and oxygen were calculated using the surface with a V_0^C (formation

energy 1.89 eV) as the reference point. Jin et al. found that the surface adsorption of molecular oxygen into V_0^C in a parallel orientation, via both oxygen atoms, is energetically more favorable than a perpendicular orientation via only one atom. Both adsorption orientations were considered here, see Figure 5 (a) and (b).
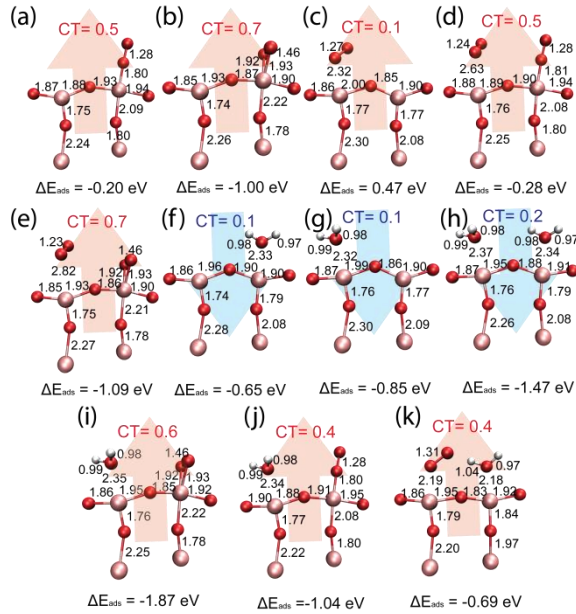

Figure 5. View of a section taken out of the optimized (001) β-WO₃ surface, (a) perpendicular adsorption of O₂ into V_0^C (b) parallel adsorption of O₂ into V_0^C, (c) adsorption of O₂ onto W5c (d) perpendicular adsorption of O₂ into V_0^C and adsorption of O₂ onto W5c. (e) parallel adsorption of O₂ into V_0^C and adsorption of O₂ onto W5c, (f) adsorption of H₂O into V_0^C (g) adsorption of H₂O onto W5c (h) adsorption of H₂O into V_0^C and adsorption of H₂O onto W5c, (i) parallel adsorption of O₂ into V_0^C and adsorption of H₂O onto W5c, (j) perpendicular adsorption of O₂ into V_0^C and adsorption of H₂O onto W5c, and (k) adsorption of O₂ onto W5c and adsorption of H₂O into V_0^C. CT denotes the charge transfer in electrons and the adsorption energy is the change referenced to the surface with a V_0^C. W atoms are colored ochre and O atoms red. If electronic charge is transferred to the surface, when compared to the surface with a terminal vacancy, then a blue arrow pointing towards the surface is used. If electronic charge is transferred from the surface, in comparison to a terminal vacancy, then the arrow is red and points upwards. Bond lengths and distances are given in Å.

The adsorption of oxygen into the vacancy is energetically favorable in both positions. In line with the findings of Jin et al., the parallel adsorption is more favorable than the perpendicular position.[48] The adsorption of oxygen on W_{5c}, however, is energetically unfavorable. The adsorption of molecular oxygen on both W_{5c} and the neighboring V_0^C is energetically close to just the respective adsorption of a single molecule in the vacancy. Similar to the results of Jin et al., climbing image nudged elastic band calculations suggest that the activation barrier for the rotation of oxygen from the perpendicular mode into the parallel mode is insignificant. Therefore, a two-step desorption process of the parallel adsorbed molecule via the perpendicular mode can be considered. The rate determining step is then likely governed by the activation energy which

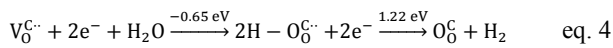equals the difference in energy of these two modes, $\Delta E=0.8$ eV.

The adsorption of molecular water on both the V_0^C and W_{5c} is found to be energetically favorable and additionally more favorable than the perpendicular adsorption of oxygen. It is favorable if water adsorbs onto the W_{5c} and oxygen adsorbs molecularly into the V_0^C, both in a parallel (-1.87 eV) and perpendicular (-1.04 eV) mode. The adsorption of molecular oxygen onto the W_{5c} and the adsorption of water into the V_0^C, is significantly less favorable (-0.69 eV). If water adsorbs onto both sites, the adsorption energy is additive, i.e. the total adsorption energy is the sum of the individual ones. These findings indicate that when considering the interaction between humidity and the WO₃ surface under real conditions, both W_{5c} and the V_0^C are possible adsorption sites.

The DRIFT spectra considered in the context of these calculations indicate that at 125 °C, the molecularly adsorbed water most likely disturbs the equilibrium of the surface with atmospheric oxygen. The detected decrease of the resistance as a result of humidity exposure at low temperatures can be explained in several ways. Considered using V_0^C as a reference, it is calculated that molecularly bound oxygen in the parallel position has a similar charge transfer as if the vacancy was healed (0.7), see Figure 5. Also in the perpendicular position, molecularly adsorbed oxygen in the vacancy removes charge from the lattice. Contrarily, the molecular adsorption of water into the vacancy is even found to push charge in, which should result in a decrease of the resistance on the surface. Additionally as a result of the adsorption of water into the surface vacancy, the overall re-oxidation process by atmospheric oxygen could be hindered. Molecularly adsorbed water onto the W_{5c} also pushes charge towards the surface. Even if water adsorbs into the W_{5c} position next to molecularly adsorbed oxygen in the vacancy, then the charge transfer to the surface is overall lower than only in the presence of the oxygen.

In the spectra at 300 °C, the bands attributed to the overtones and combinations of the WO₃ lattice, 2063 and 1854 cm⁻¹, are increasing. At this temperature, the bands attributed to molecularly adsorbed water are barely visible. This, in addition to the detected increase of the resistance, indicates that the tungsten oxide surface is more oxidized in the presence of humidity than in dry synthetic air. An explanation for the spectrum would be the healing of the oxygen vacancies by water followed by the subsequent release of hydrogen. In their work, Teusch and Klüner theoretically examined the splitting of water on WO₃. [22] In their suggested path, the formation of hydroxyl groups is an intermediary step. Their work was however only theoretical. Uniquely, this paper combines experimental results with calculations in order to understand the temperature dependent evolution of hydrogen from humidity. In the DRIFT spectra, unlike other metal oxides, e.g. SnO₂[32], there is no hydroxyl group formation visible at any temperature. This experimental result indicates that after adsorption of water molecularly into a vacancy (dominantly visible at low temperatures) the direct oxidation of the surface takes place without the formation of intermediaries (e.g. hydroxyl groups). The experimental measurements were, however, done under very high humidity conditions (10 %RH).In their study, Teusch and Klüner, only consider the W_{5c} as an adsorption site for water. Based on the findings here, and the work of Albanese et al., it is clear that adsorption onto V_0^C must also be considered. It is therefore possible that in reality, the level of

water adsorption on the surface is more than the monolayer (all W_{5c} covered) examined by Teusch and Klüner. [22] In this case, the evolution of hydrogen, for example could be a result of an interaction between neighboring water molecules. A large theoretical study coupled with additional measurements is currently being run to further examine the role of surface coverage on the mechanism.

In summary, if the temperature study using DRIFT spectroscopy and DC resistance measurements is considered in the context of the literature and the DFT calculations, the following surface reactions can be identified. At low temperatures water can adsorb molecularly into V_O^C or onto W_{5c}. This results in a significant decrease of the resistance, because the re-oxidation of the surface through atmospheric oxygen is hindered and molecularly adsorbed water pushes charge into the surface. At 200 °C, the degree of molecular water adsorption and the subsequent surface oxidation/ release of hydrogen are similar. As a result the change of the film's resistance is also low. In this case, no change of the bands attributed to tungsten-oxygen bonds is visible in the DRIFT spectra. Additionally, the bands associated with adsorbed water are lower than at 125 °C. At 300 °C, hydrogen is released from the molecularly adsorbed water. The formation of intermediary hydroxyl groups is not visible in the DRIFT spectra. An overall reaction can be formulated as

$$V_O^{C\cdot\cdot} + 2e^- + H_2O \xrightarrow{-0.65\ eV} 2H - O_O^{C\cdot\cdot} + 2e^- \xrightarrow{1.22\ eV} O_O^C + H_2 \qquad \text{eq. 4}$$

where 1.22 eV is the energy required to split an adsorbed water mocule to form hydrogen. The adsorption of hydrogen on the reoxidized surface is depicted in Figure 6. It is important to note that this process doesn't cease as the surface is in constant equilibrium with the atmosphere. Namely, oxygen vacancies are created and healed by de- and adsorption of oxygen as described by the following reaction:[49]
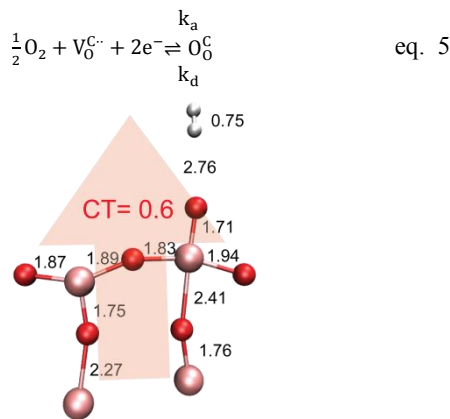
$$\tfrac{1}{2}O_2 + V_O^{C\cdot\cdot} + 2e^- \underset{k_d}{\overset{k_a}{\rightleftharpoons}} O_O^C \qquad \text{eq. 5}$$

Figure 6. View of a section taken out of the optimized (001) β-WO₃ surface on which a surface vacancy was healed and hydrogen was released.

In order to verify the evolution of hydrogen at 300 °C, catalytic conversion measurements were done. One gram of WO₃-powder was heated to 300 °C in a reactor. The powder was first exposed to dry synthetic air and then to 10% RH. The exhaust was monitored using a highly sensitive H_2 sensor (TGS2600, Figaro Engineering Inc., Japan). [50]
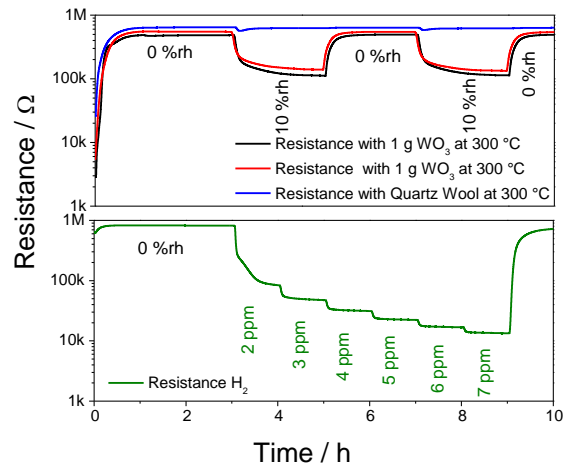
Figure 7. The resistance of the TGS2600 sensor. The red and black lines are measurements done of a heated gram of WO₃. The blue line is the same measurement done without WO₃ (heated empty tube). The green line is the resistance change during exposure to different concentrations of hydrogen taken from a gas bottle.

The sensor's response during the exhaust measurement is shown in Figure 7. The red and black lines are measurements done with one gram of WO₃ in the reactor heated to 300 °C. The measurements were done twice with two different samples (fresh powder) to show that the results are reproducible and that the process is reversible. The blue line is the same measurement done without WO₃ (only a heated tube) to show that the sensor is not responding to residual humidity. The green line is a measurement done during gas pulses from a hydrogen bottle, in order to show the response of the sensor to hydrogen. This shows that hydrogen is not eliminated by the molecular sieve or the silica gel. It also indicates that based on the response of the TGS2600 to the exhaust, that the reaction between WO₃ and humidity results in a production of over 1 ppm of H_2. The measurement indicates that the hydrogen evolution is constant and that once humidity is removed the process stops. Repetition of the measurement using the same sample showed the same response indicating that the process is fully reversible. Overall, the presented results reveal that at 300 °C water is split on the surface of WO₃ and there is a constant evolution of hydrogen. This process appears to be of catalytic nature and the proposed mechanism is shown in Figure 8.
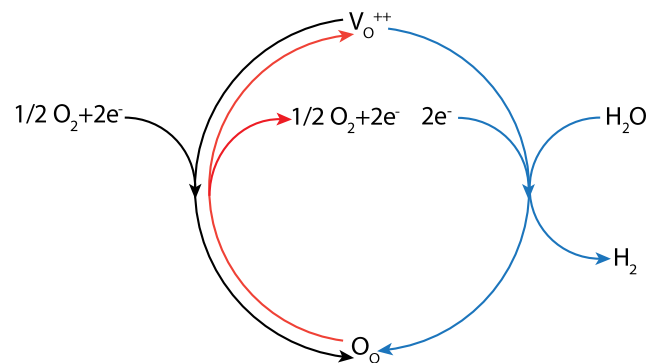
Figure 8. Proposed catalytic cycle of the continuous water splitting on the WO₃ surface.

Conclusion

The value of the systematic study presented here is twofold. It is remarkable that the evolution of hydrogen from humidity was identified under extremely mild conditions, 300 °C in humidity. In addition, with the gained insights into the reaction mechanism, the interference of humidity in the various applications of WO_3 can now be understood. For example, it is probable that the sensor signal of the chemiresistive WO_3 gas sensors operated at 300 °C decreases to oxidizing gases because humidity itself also oxidizes the surface. The findings support the explanation of Gavrilyuk that adsorbed water decreases the photochromism of pure WO_3 by blocking the surface adsorption centers.[6] The findings, however, also give an explanation for the remarkable promotion of the oxidation reaction rate by humidity described by Matsuyama et al. for fiber optic gas sensors based on noble loaded WO_3.[4] The remarkable ability of water to oxidize the surface, may also offer an alternative explanation for the enhanced memristive behavior of WO_3 in the presence of humidity. In other words, instead of the mechanism proposed by Zhou et al., one driven by the incorporation of oxygen from the water molecules is probable. A similar mechanism was proposed by Heisig et al. for $SrTiO_3$.[51] Additionally, although recently there has been a high level of interest in modeling the surface reaction with humidity, this paper identifies several aspects that must be additional considered, e.g. higher level of water coverage and competing reaction with atmospheric oxygen.

ASSOCIATED CONTENT

Supporting Information. DRIFT spectra during 10 %RH. Temperature dependent XRD of the film based on SA. Operando XRD of a SA sensor operated at 125 °C during an initial 3 h exposure to dry synthetic air and then to 90 %RH.

AUTHOR INFORMATION

Corresponding Author

* nb@ipc.uni-tuebingen.de; Tel.: +49 7071 29 78761

Author Contributions

The manuscript was written through contributions of all authors. All authors have given approval to the final version of the manuscript.

ACKNOWLEDGMENT

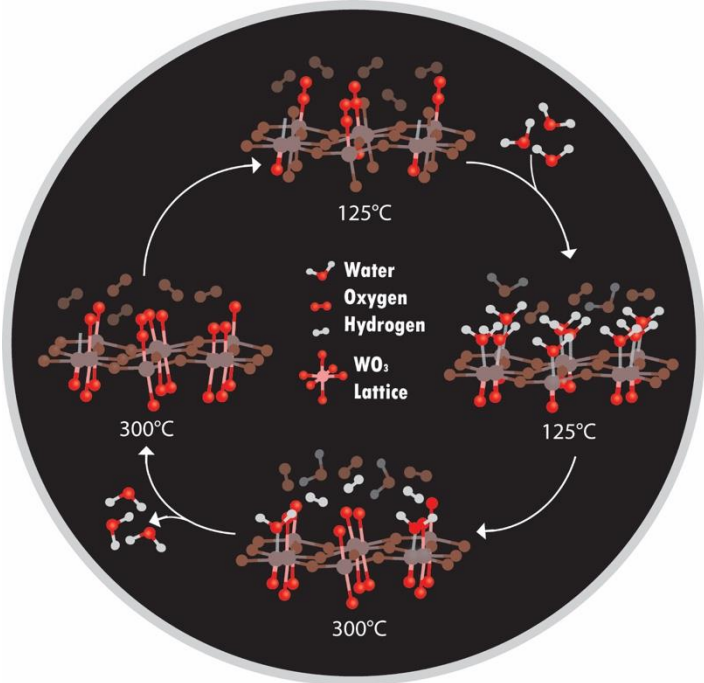## REFERENCES.

(1)   Deb, S. K. A Novel Electrophotographic System. *Appl. Opt.* **1969**, No. 8, 192–195.

(2)   Burkhardt, S.; Elm, M. T.; Lani-wayda, B.; Klar, P. J. In Situ Monitoring of Lateral Hydrogen Diffusion in Amorphous and Polycrystalline WO_3 Thin Films. **2018**, *1701587*, 1–9. https://doi.org/10.1002/admi.201701587.

(3)   Sekimoto, S.; Nakagawa, H.; Okazaki, S.; Fukuda, K.; Asakura, S.; Shigemori, T.; Takahashi, S. Fiber-Optic Evanescent-Wave Hydrogen Gas Sensor Using Palladium-Supported Tungsten Oxide. *Sensors Actuators, B Chem.* **2000**, *66* (1), 142–145. https://doi.org/10.1016/S0925-4005(00)00330-0.

(4)   Matsuyama, N.; Okazaki, S.; Nakagawa, H.; Sone, H.; Fukuda, K. Response Kinetics of a Fiber-Optic Gas Sensor Using Pt / WO_3 Thin Film to Hydrogen. *Thin Solid Films* **2009**, *517* (16), 4650–4653. https://doi.org/10.1016/j.tsf.2009.01.126.

(5)   Xi, Y.; Zhang, Q.; Cheng, H. Mechanism of Hydrogen Spillover on WO_3 (001) and Formation of H_xWO_3 (X=0.125, 0.25, 0.375, and 0.5). *J. Phys. Chem. C* **2014**, *3* (001), 494–501.

(6)   Gavrilyuk, A. I. Aging of the Nanosized Photochromic WO_3 Films and the Role of Adsorbed Water in the Photochromism. *Appl. Surf. Sci.* **2016**, *364*, 498–504. https://doi.org/10.1016/j.apsusc.2015.12.195.

(7)   Wang, S.; Fan, W.; Liu, Z.; Yu, A.; Jiang, X. Advances on Tungsten Oxide Based Photochromic Materials: Strategies to Improve Their Photochromic Properties. *J. Mater. Chem. C* **2018**, *6* (2), 191–212. https://doi.org/10.1039/c7tc04189f.

(8)   Zhou, Y.; Peng, Y.; Yin, Y.; Zhou, F.; Liu, C.; Ling, J.; Lei, L.; Zhou, W.; Tang, D. Modulating Memristive Performance of Hexagonal WO_3 Nanowire by Water-Oxidized Hydrogen Ion Implantation. *Sci. Rep.* **2016**, *6* (August), 1–9. https://doi.org/10.1038/srep32712.

(9)   Brattain, W. H.; Bardeen, J. Surface Properties of Germanium. *Bell Labs Tech. J.* **1953**, *32* (1), 1–41.

(10)   Seiyama, T.; Kato, A.; Fujishi, K.; Nagatani, M. A New Detector for Gaseous Components Using Semiconductive Thin Films. *Anal. Chem.* **1962**, 2–3. https://doi.org/https://doi.org/10.1021/ac60191a001.

(11)   Taguchi, N. Gas-Detecting Device. US3695848, 1971.

(12)   Barsan, N.; Weimar, U. Conduction Model of Metal Oxide Gas Sensors. *J. Electroceramics* **2001**, *7* (3), 143–167. https://doi.org/10.1023/A:1014405811371.

(13)   Heiland, G.; Kohl, D. Physical and Chemical Aspects of Oxidic Semiconductor Gas Sensors. In *Chemical Sensor Technology*; Seiyama, T., Ed.; Elsevier Science, 1992; pp 43–88.

(14)   Staerz, A.; Somacescu, S.; Epifani, M.; Kida, T.; Weimar, U.; Barsan, N. WO3 Based Gas Sensors: Identifying Inherent Qualities and Understanding the Sensing Mechanism. *Acs Sensors* **2020**. https://doi.org/10.1021/acssensors.0c00113.

(15)   Staerz, A.; Berthold, C.; Russ, T.; Wicker, S.; Weimar, U.; Barsan, N. The Oxidizing Effect of Humidity on WO3 Based Sensors. *Sensors Actuators B Chem.* **2016**, *237*, 54–58. https://doi.org/10.1016/j.snb.2016.06.072.

(16)   Pokhrel, S.; Simion, C. E.; Teodorescu, V. S.; Barsan, N.; Weimar, U. Synthesis, Mechanism, and Gas-Sensing Application of Surfactant Tailored Tungsten Oxide Nanostructures. *Adv. Funct. Mater.* **2009**, *19*, 1767–1774. https://doi.org/10.1002/adfm.200801171.

(17)   Utembe, S. R.; Hansford, G. M.; Sanderson, M. G.; Freshwater, R. a; Pratt, K. F. E.; Williams, D. E.; Cox, R. a; Jones, R. L. An Ozone Monitoring Instrument Based on the Tungsten Trioxide Semiconductor. *Sensors and Actuators B-Chemical* **2006**, *114* (1), 507–512. https://doi.org/DOI 10.1016/j.snb.2005.04.049.

(18)   Neri, G. First Fifty Years of Chemoresistive Gas Sensors. *Chemosensors* **2015**, *3* (1), 1–20. https://doi.org/10.3390/chemosensors3010001.

(19)   Pokhrel, S.; Simion, C. E.; Teodorescu, V. S.; Barsan, N.; Weimar, U. Synthesis, Mechanism, and Gas-Sensing Application of Surfactant Tailored Tungsten Oxide Nanostructures. *Adv. Funct. Mater.* **2009**, *19* (11), 1767–1774. https://doi.org/10.1002/adfm.200801171.

(20)   Daeneke, T.; Dahr, N.; Atkin, P.; Clark, R. M.; Harrison, C. J.; Pillai, N.; Zhang, B. Y.; Zavabeti, A.; Ippolito, S. J.; Berean, K. J.; Ou, J. Z.; Strano, M. S.; Kalantar-zadeh, K. Surface Water Dependent Properties of Sulfur- Rich Molybdenum Sulfides: Electrolyteless Gas Phase Water Splitting. **2017**, No. Iv. https://doi.org/10.1021/acsnano.7b01632.

(21)   Albanese, E.; Di Valentin, C.; Pacchioni, G. H_2O Adsorption on WO_3 and WO_{3-x} (001) Surfaces. *ACS Appl. Mater. Interfaces* **2017**, *9* (27), 23212–23221. https://doi.org/10.1021/acsami.7b06139.

(22)   Teusch, T.; Klüner, T. Understanding the Water Splitting

Mechanism on WO3(001) - A Theoretical Approach. *J. Phys. Chem. C* **2019**, *123* (46), 28233–28240. https://doi.org/10.1021/acs.jpcc.9b08268.

(23) Kishore, R.; Cao, X.; Zhang, X.; Bieberle-Hütter, A. Electrochemical Water Oxidation on WO3 Surfaces: A Density Functional Theory Study. *Catal. Today* **2019**, *321–322* (February 2018), 94–99. https://doi.org/10.1016/j.cattod.2018.02.030.

(24) Mao, Y.; Gao, Y.; Dong, W.; Wu, H.; Song, Z.; Zhao, X.; Sun, J.; Wang, W. Hydrogen Production via a Two-Step Water Splitting Thermochemical Cycle Based on Metal Oxide – A Review. *Appl. Energy* **2020**, *267* (October 2019), 114860. https://doi.org/10.1016/j.apenergy.2020.114860.

(25) Abanades, S. Metal Oxides Applied to Thermochemical Water-Splitting for Hydrogen Production Using Concentrated Solar Energy. *ChemEngineering* **2019**, *3* (3), 63. https://doi.org/10.3390/chemengineering3030063.

(26) Berthold, C.; Bjeoumikhov, A.; Brügemann, L. Fast XRD2 Microdiffraction with Focusing X-Ray Microlenses. *Part. Part. Syst. Charact.* **2009**, *26*, 107–111. https://doi.org/10.1002/ppsc.200800038.

(27) Olinger, J. M.; Griffiths, P. R. Quantitative Effects of an Absorbing Matrix on Near-Infrared Diffuse Reflectance Spectra. *Anal. Chem.* **1988**, *60* (21), 2427–2428. https://doi.org/10.1021/ac00172a022.

(28) Sirita, J.; Phanichphant, S.; Meunier, F. C. Quantitative Analysis of Adsorbate Concentrations by Diffuse Reflectance FT-IR. *Anal. Chem.* **2007**, *79* (0), 3912–3918. https://doi.org/10.1021/ac0702802.

(29) Kresse, G.; Hafner, J. Ab Initio Molecular-Dynamics Simulation of the Liquid-Metal–Amorphous-Semiconductor Transition in Germanium. *Phys. Rev. B* **1994**, *49* (20), 14251–14269. https://doi.org/10.1103/PhysRevB.49.14251.

(30) Kresse, G.; Furthmüller, J. Efficiency of Ab-Initio Total Energy Calculations for Metals and Semiconductors Using a Plane-Wave Basis Set. *Comput. Mateials Sci.* **1996**, *6*, 15–50. https://doi.org/http://dx.doi.org/10.1016/0927-0256(96)00008-0.

(31) Perdew, J. P.; Ernzerhof, M.; Burke, K. Rationale for Mixing Exact Exchange with Density Functional Approximations. *J. Chem. Phys.* **1996**, *105* (22), 9982–9985. https://doi.org/10.1063/1.472933.

(32) Wicker, S.; Guiltat, M.; Weimar, U.; Hémeryck, A.; Barsan, N. Ambient Humidity Influence on CO Detection with SnO2 Gas Sensing Materials. A Combined DRIFTS/DFT Investigation. *J. Phys. Chem. C* **2017**, *121* (45), 25064–25073. https://doi.org/10.1021/acs.jpcc.7b06253.

(33) Joubert, D. From Ultrasoft Pseudopotentials to the Projector Augmented-Wave Method. *Phys. Rev. B - Condens. Matter Mater. Phys.* **1999**, *59* (3), 1758–1775. https://doi.org/10.1103/PhysRevB.59.1758.

(34) Blochl, P. E. Projector Augmented-Wave Method. **1994**, *50* (24).

(35) Monkhorst, H. J.; Pack, J. D. Special Points for Brillouin-Zone Integrations. *Phys. Rev. B* **1976**, *13* (12), 5188–5192. https://doi.org/10.1103/PhysRevB.13.5188.

(36) Tang, W.; Sanville, E.; Henkelman, G. A Grid-Based Bader Analysis Algorithm without Lattice Bias. *J. Phys. Condens. Matter* **2009**, *21* (084204), 1–7. https://doi.org/10.1088/0953-8984/21/8/084204.

(37) Humphrey, W.; Dalke, A.; Schulten, K. VMD: Visual Molecular Dynamics. *J. Mol. Graph.* **1996**, *14* (1), 33–38. https://doi.org/10.1016/0263-7855(96)00018-5.

(38) Persistence of Vision Raytracer. Persistence of Vision Pty. Ltd. 2004.

(39) Staerz, A. Methods for Expanding the Diversity in the Response of Metal Oxide Based Gas Sensors, University of Tuebingen, 2019.

(40) Kanan, S. M.; Lu, Z.; Cox, J. K.; Bernhardt, G.; Tripp, C. P. Identification of Surface Sites on Monoclinic WO3 Powders by Infrared Spectroscopy. *Langmuir* **2002**, *18* (5), 1707–1712. https://doi.org/10.1021/la011428u.

(41) Roedel, E.; Urakawa, A.; Kureti, S.; Baiker, A. On the Local Sensitivity of Different IR Techniques: Ba Species Relevant in NO(x) Storage-Reduction. *Phys. Chem. Chem. Phys.* **2008**, *10* (40), 6190–6198. https://doi.org/10.1039/b808529c.

(42) Daniel, M. F.; Desbat, B.; Lassegues, J. C. Infrared and Raman Study of WO3 Tungsten Trioxide and WO3x H2O Tungsten Trioxide Hydrates Trioxides. *J. Solid State Chem.* **1987**, *247* (2), 235–247. https://doi.org/10.1016/0022-4596(87)90359-8.

(43) Arai, M.; Hayashi, S.; Yamamoto, K. Raman Studies of Phase Transitions in Gas-Evaporated WO3 Microcrystals. *Solid State Commun.* **1990**, *75* (7), 613–616.

(44) Righettoni, M.; Pratsinis, S. E. Annealing Dynamics of WO3 by in Situ XRD. *Mater. Res. Bull.* **2014**, *59*, 199–204. https://doi.org/10.1016/j.materresbull.2014.07.018.

(45) Salje, E. The Orthorhombic Phase of WO3. *Acta Cryst. B* **1977**, *33* (1), 574–577. https://doi.org/10.1107/S0567740877004130.

(46) Loopstra, B. O.; Boldrini, P. Neutron Diffraction Inverstigation of WO3. *Acta Cryst . B.* **1966**, No. 21. https://doi.org/https://doi.org/10.1107/S0365110X66002469.

(47) Lu, D. Y.; Chen, J.; Chen, H. J.; Gong, L.; Deng, S. Z.; Xu, N. S.; Liu, Y. L. Raman Study of Thermochromic Phase Transition in Tungsten Trioxide Nanowires. *Appl. Phys. Lett.* **2007**, *90* (4), 96–99. https://doi.org/10.1063/1.2435616.

(48) Jin, H.; Zhou, H.; Zhang, Y. Insight into the Mechanism of CO Oxidation on WO3(001) Surfaces for Gas Sensing: A DFT Study. *Sensors* **2017**, *17* (1898), 1–12. https://doi.org/10.3390/s17081898.

(49) Gillet, M.; Lemire, C.; Gillet, E.; Aguir, K. The Role of Surface Oxygen Vacancies upon WO3 Conductivity. *Surf. Sci.* **2003**, *532–535*, 519–525. https://doi.org/10.1016/S0039-6028(03)00477-1.

(50) Figaro Engineering Inc. *Technical Information for TGS2600*; Osaka, Japan, 2004.

(51) Heisig, T.; Baeumer, C.; Gries, U. N.; Mueller, M. P.; La Torre, C.; Luebben, M.; Raab, N.; Du, H.; Menzel, S.; Mueller, D. N.; Jia, C. L.; Mayer, J.; Waser, R.; Valov, I.; De Souza, R. A.; Dittmann, R. Oxygen Exchange Processes between Oxide Memristive Devices and Water Molecules. *Adv. Mater.* **2018**, *30* (29), 1–7. https://doi.org/10.1002/adma.201800957.

(52) Wu, Y.; Chan, M. K. Y.; Ceder, G. Prediction of Semiconductor Band Edge Positions in Aqueous Environments from First Principles. *Phys. Rev. B - Condens. Matter Mater. Phys.* **2011**, *83* (23), 1–7. https://doi.org/10.1103/PhysRevB.83.235301.

(53) Szymanski, J. T.; Roberts, A. C. The Crystal Structure of Tungstite, WO3-H2O. *Can. Mineral.* **1984**, *22* (July), 681–688.

(54) Günter, J. R.; Amberg, M.; Schmalle, H. Direct Synthesis and Single Crystal Structure Determination of Cubic Pyrochlore-Type Tungsten Trioxide Hemihydrate, WO3 · 0.5H2O. *Mater. Res. Bull.* **1989**, *24* (3), 289–292. https://doi.org/10.1016/0025-5408(89)90214-6 Get.

(55) Gerand, B.; Nowogrocki, G.; Figlarz, M. A New Tungsten Trioxide Hydrate, WO3 · 1/3H2O: Preparation, Characterization, and Crystallographic Study. *J. Solid State Chem.* **1981**, *38* (3), 312–320. https://doi.org/10.1016/0022-4596(81)90062-1.

(56) Loopstra, B. O.; Rietveld, H. M. Further Refinement of the Structure of WO3. *Acta Crystallogr. Sect. B Struct. Crystallogr. Cryst. Chem.* **1969**, *25* (7), 1420–1421. https://doi.org/10.1107/S0567740869004146.

TOC graphic
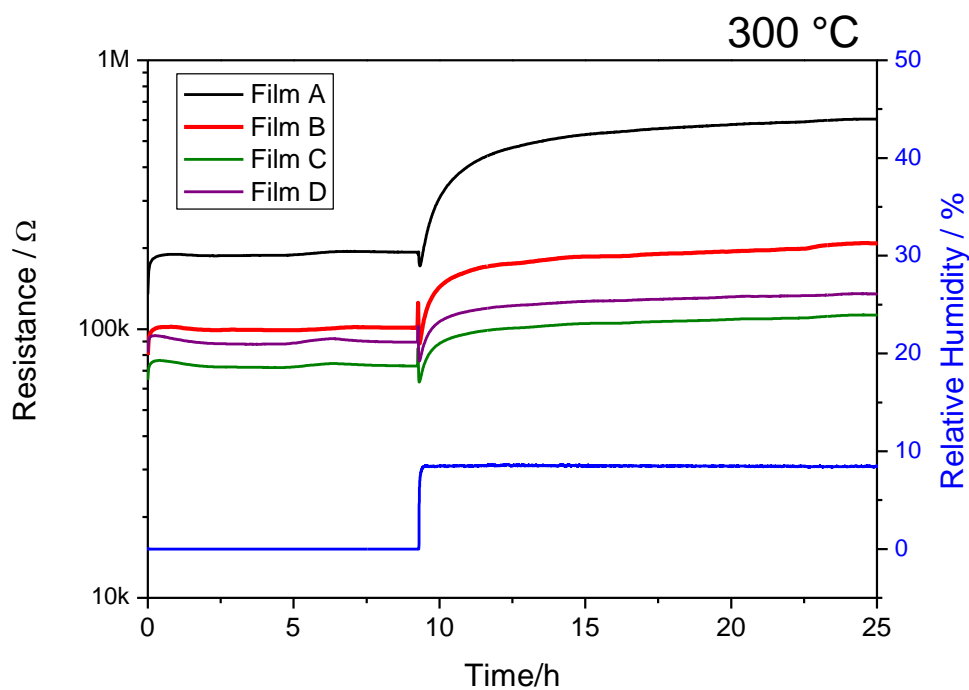
SUPPORTING INFORMATION

THERMAL WATER SPLITTING ON THE WO₃ SURFACE-EXPERIMENTAL PROOF

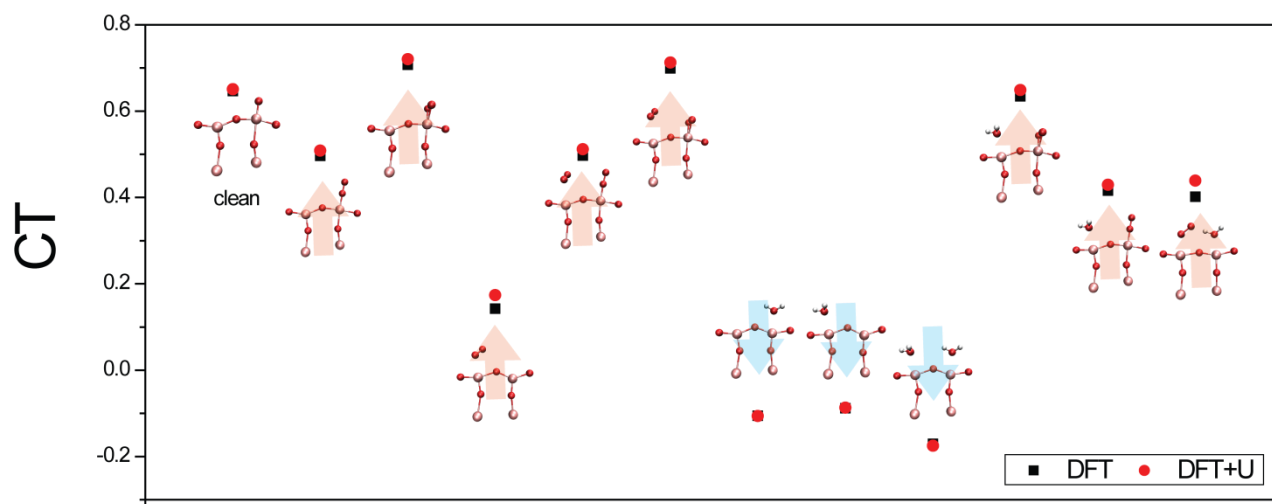Anna Staerz[1], Arne Kobald[1], Tamara Russ[1], Udo Weimar[1], Anne Hémeryck[2] and Nicolae Barsan[1,*]

[1]Faculty of Science, Department of Chemistry, Institute of Physical and Theoretical Chemistry, Tuebingen University, Auf der Morgenstelle 15, 72076 Tuebingen, Germany

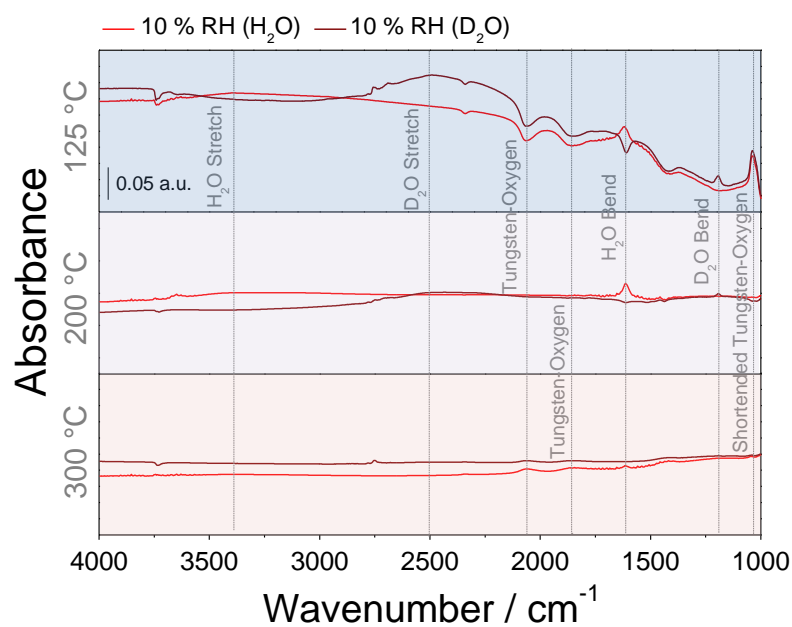[2]LAAS-CNRS, Université de Toulouse, CNRS, 31400 Toulouse, France

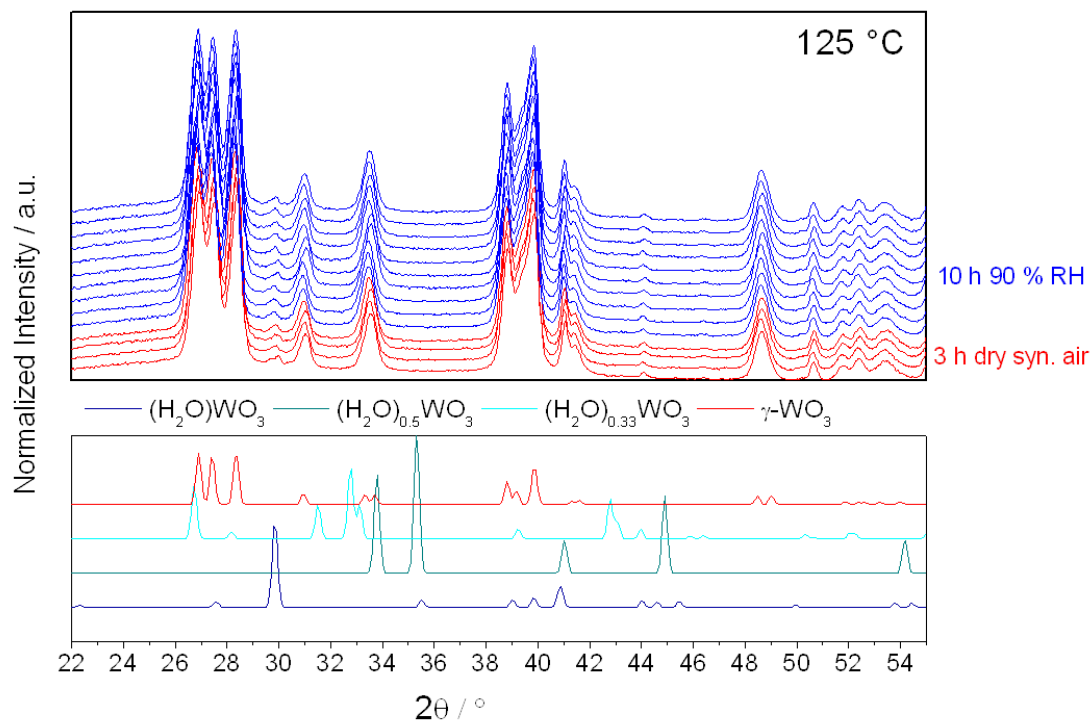*Corresponding Author: nb@ipc.uni-tuebingen.de

S1. The resistance measurements of four identical WO₃ films operated at 300 °C and the simultaneously measured humidity concentration in the exhaust gas (monitored with a HYT939 humidity sensor).
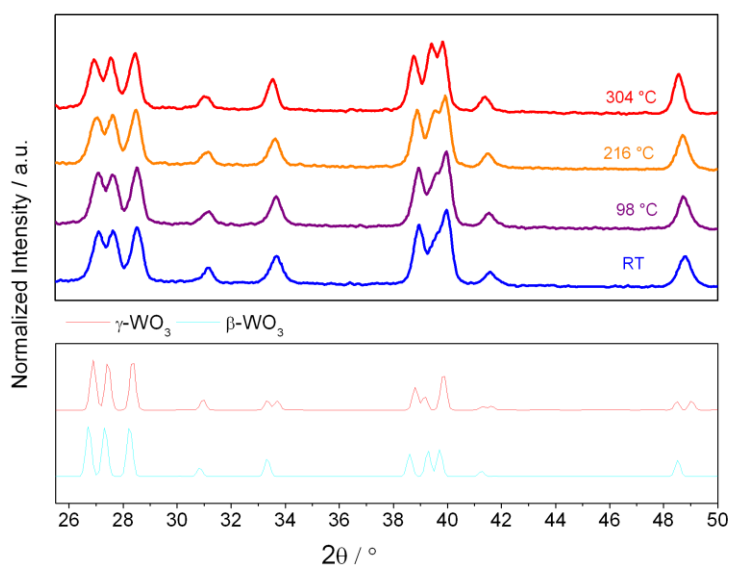
S2. To account for strongly self interacting electrons the DFT+U approach was also considered here. Similar to Kishore et al. the Hubbard U parameter for W was chosen as 2.0 eV.[1,2] However, the charge transfers were found to not differ significantly.

S3. Total DRIFT spectra of the film during exposure to H_2O and subsequent exposure to D_2O.

S4. Operando XRD of a SA sensor operated at 125 °C during an initial 3 h exposure to dry synthetic air and then to 90 %RH. The attained diffractograms are compared to those of $(H_2O)WO_3$[3], $(H_2O)_{0.5}WO_3$[4], $(H_2O)_{0.33}WO_3$[5] and γ-WO_3[6].

S5. Temperature dependent XRD of the film based on SA. The attained diffractograms are compared to those of β-WO_3[7] and γ-WO_3[6].

S-3

REFERENCES.

(1)   Kishore, R.; Cao, X.; Zhang, X.; Bieberle-Hütter, A. Electrochemical Water Oxidation on WO3 Surfaces: A Density Functional Theory Study. *Catal. Today* **2019**, *321–322* (February 2018), 94–99. https://doi.org/10.1016/j.cattod.2018.02.030.

(2)   Wu, Y.; Chan, M. K. Y.; Ceder, G. Prediction of Semiconductor Band Edge Positions in Aqueous Environments from First Principles. *Phys. Rev. B - Condens. Matter Mater. Phys.* **2011**, *83* (23), 1–7. https://doi.org/10.1103/PhysRevB.83.235301.

(3)   Szymanski, J. T.; Roberts, A. C. The Crystal Structure of Tungstite, WO_3-H_2O. *Can. Mineral.* **1984**, *22* (July), 681–688.

(4)   Günter, J. R.; Amberg, M.; Schmalle, H. Direct Synthesis and Single Crystal Structure Determination of Cubic Pyrochlore-Type Tungsten Trioxide Hemihydrate, $WO_3 \cdot 0.5H_2O$. *Mater. Res. Bull.* **1989**, *24* (3), 289–292. https://doi.org/10.1016/0025-5408(89)90214-6 Get.

(5)   Gerand, B.; Nowogrocki, G.; Figlarz, M. A New Tungsten Trioxide Hydrate, $WO_3 \cdot 1/3H_2O$: Preparation, Characterization, and Crystallographic Study. *J. Solid State Chem.* **1981**, *38* (3), 312–320. https://doi.org/10.1016/0022-4596(81)90062-1.

(6)   Loopstra, B. O.; Rietveld, H. M. Further Refinement of the Structure of WO_3. *Acta Crystallogr. Sect. B Struct. Crystallogr. Cryst. Chem.* **1969**, *25* (7), 1420–1421. https://doi.org/10.1107/S0567740869004146.

(7)   Salje, E. The Orthorhombic Phase of WO_3. *Acta Cryst. B* **1977**, *33* (1), 574–577. https://doi.org/10.1107/S0567740877004130.